

Spin-orbit coupling induced magnetic anisotropy and large spin wave gap in NaOsO₃

Avinash Singh,^{1,2} Shubhajyoti Mohapatra,¹ Churna Bhandari,² and Sashi Satpathy²

¹*Department of Physics, Indian Institute of Technology, Kanpur - 208016, India*

²*Department of Physics and Astronomy,
University of Missouri, Columbia, MO 65201*

(Dated: December 3, 2024)

The role of spin-orbit coupling and Hund's rule coupling on magnetic ordering, anisotropy, and excitations are investigated within a minimal three-orbital model for the $5d^3$ compound NaOsO₃. Asymmetry between the magnetic moments for the xy and xz, yz orbitals, arising from the hopping asymmetry generated by the OsO₆ octahedral tilting and rotation, together with the weak correlation effect, are shown to be crucial for the large SOC induced magnetic anisotropy and spin wave gap observed in this compound. The tetragonal distortion-induced orbital energy offset ϵ_{xy} is also found to contribute significantly to the magnetic anisotropy energy.

I. INTRODUCTION

The strongly spin-orbit coupled $5d^3$ orthorhombic structured osmium compound NaOsO_3 , with nominally three electrons in the Os t_{2g} sector orbitals, exhibits several novel electronic and magnetic properties. These include a G-type antiferromagnetic (AFM) structure for NaOsO_3 with spins oriented along the c axis,¹ a significantly reduced magnetic moment (from $3\mu_B$ in the localized-spin picture for the half-filled t_{2g} sector) of $\sim 1\mu_B$ as measured from neutron scattering and ascribed to itinerant-electron behavior due to hybridization between Os d and O p orbitals,¹ a continuous metal-insulator transition (MIT) that coincides with the AFM transition ($T_N = T_{\text{MIT}} = 410$ K) as seen in neutron and x-ray scattering,¹ and a large spin wave energy gap of 58 meV as seen in resonant inelastic X-ray scattering (RIXS) measurements indicating strong magnetic anisotropy.²

Neutron scattering and RIXS studies of the magnetic excitation spectrum have also revealed large spin wave gap in the frustrated type I AFM ground state of the double perovskites Ba_2YOsO_6 , $\text{Sr}_2\text{ScOsO}_6$, $\text{Ca}_3\text{LiOsO}_6$,³⁻⁵ highlighting the importance of SOC induced anisotropy despite the nominally orbitally-quenched ions in the $5d^3$ and $4d^3$ systems. For the pyrochlore compound $\text{Cd}_2\text{Os}_2\text{O}_7$ also, neutron diffraction and RIXS measurements have directly probed the $5d$ electrons responsible for the magnetic order and MIT in both the metallic and insulating regimes.⁶

Investigations of the electronic and magnetic properties using first-principle calculations have been carried out for the orthorhombic perovskite NaOsO_3 ,^{7,8} related osmium based perovskites AOsO_3 ($A=\text{Ca},\text{Sr},\text{Ba}$),⁹ and double perovskites $\text{Ca}_2\text{CoOsO}_6$ and $\text{Ca}_2\text{NiOsO}_6$.¹⁰ Density functional theory (DFT) calculations have shown that the magnetic moment is strongly reduced to nearly $1\mu_B$ (essentially unchanged by SOC) due to itineracy resulting from the strong hybridization of the t_{2g} orbitals with the oxygen $2p$ orbitals, which is significantly affected by the structural distortion.⁸ Furthermore, from total energy calculations for different spin orientations with SOC included, the easy axis was determined as $\langle 001 \rangle$,⁸ as also observed by Calder *et al.*,¹ with large energy cost for orientation along the $\langle 010 \rangle$ axis and very small energy difference between orientations along the nearly symmetrical a and c axes.

The OsO_6 octahedral rotation and tilting in NaOsO_3 result in moderate bandwidth reduction within the t_{2g} manifold, which has been noted as an important contributing factor

to the marginally gapped AFM state. A detailed study of the electronic band structure of NaOsO_3 has been carried out recently within a three-orbital model and compared with DFT results for both the undistorted and distorted structures.¹¹ A slightly orbitally asymmetric bandwidth reduction along with a slight moment disparity ($m_{yz}, m_{xz} > m_{xy}$) was obtained for the distorted structure.

Although weak correlation effects are central to the Slater scenario for both NaOsO_3 and $\text{Cd}_2\text{Os}_2\text{O}_7$ which exhibit continuous MIT concomitant with three dimensional AFM ordering, magnetic interactions and excitations in both compounds have been studied only within the phenomenological localized spin picture. Investigation of the strong SOC induced magnetic anisotropy and spin wave gap within the itinerant electron picture in terms of a weakly correlated minimal three-orbital model is therefore of particular interest. Indeed, for the iridate compounds, recent study of magnetic excitations in terms of the itinerant electron approach have provided a microscopic understanding of features such as the strong zone boundary spin wave dispersion in the single-layer compound and the large spin wave gap in the bilayer compound, as observed in RIXS studies, in terms of characteristic weak correlation effects in the $5d$ systems.¹²

Focussing on the SOC induced magnetic anisotropy in this paper, we will therefore investigate: i) the key features required in a minimal three-orbital model within the t_{2g} sector in order to understand the SOC induced magnetic anisotropy and easy axis, ii) role of the Hund's coupling term on the magnetic order, and (iii) magnetic excitations and the large SOC induced spin wave anisotropy gap. The Hund's rule coupling term will be shown to play a particularly important role in view of the SOC induced intra-site magnetic frustration (similar to that in the triangular-lattice AFM) involving the three magnetic moments S_μ for the three orbitals $\mu = yz, xz, xy$ on the same site.

The structure of this paper is as follows. Starting with a minimal three-orbital model with strong spin-orbit coupling (Sec. II) and brief discussion of the band and staggered field terms in the three-orbital basis, the SOC induced magnetic anisotropy is studied in Sec. III in terms of the AFM state energy at half filling ($n = 3$) for different orientations of the staggered field. Here the staggered fields (and therefore the orbital magnetic moments m_μ) for the three orbitals $\mu = yz, xz, xy$ are assumed to be parallel. As this orbitally collinear AFM state is seen to be unstable (without Hund's coupling) in a spin wave analysis, an orbitally canted AFM state is studied in Sec. IV, motivated by the SOC induced anisotropic (orbital-

Kitaev) spin interactions and intra-site magnetic frustration effect obtained in a strong coupling analysis (Appendix A). Magnetic excitations are studied in Sec. V, highlighting the non-trivial role of Hund's coupling in overcoming the magnetic frustration and stabilizing the orbitally collinear AFM state and thus activating the SOC induced magnetic anisotropy. Finally, connecting with the earlier electronic band structure investigation, conclusions are presented in Sec. VI.

II. THREE ORBITAL MODEL AND MAGNETIC ORDERING

The electronic and magnetic behaviour of NaOsO₃ as discussed above indicates a complex interplay between SOC, structural distortion, magnetic ordering, Hund's rule coupling, and weak correlation effect. While strong SOC would favor spin-orbital entangled states energetically separated into the $J = 1/2$ doublet and $J = 3/2$ quartet, strong Hund's rule coupling would favor the spin-disentangled, high-spin nominally $S = 3/2$ state in the half-filled system with three electrons per Os ion. In the high-spin state, Hund's rule coupling also effectively enhances the local exchange field, supporting the weak correlation term in the formation of the AFM state. The enhanced local exchange field energetically separates the spin up and down states, thus self consistently suppressing the SOC.

A detailed study of the electronic band structure of NaOsO₃ has been carried out recently for both the undistorted and distorted structures.¹¹ Effects of the structural distortion associated with the OsO₆ octahedral rotation and tilting on the electronic band structure were investigated using the density functional theory (DFT) and reproduced within a three-orbital model. Comparison of the essential features of the DFT band structures with the three-orbital model for both the undistorted (cubic) and distorted (orthorhombic) structures provided insight into the orbital and directional asymmetry in the electron hopping terms resulting from the structural distortion. The orbital mixing terms obtained in the transformed hopping Hamiltonian resulting from the octahedral rotations were shown to account for the fine features in the DFT band structure. Study of staggered magnetization indicated weak coupling behavior, suggesting relevance of Slater mechanism in the magnetic transition. A slightly orbitally asymmetric bandwidth reduction, as indicated by the slight moment disparity ($m_{yz}, m_{xz} > m_{xy}$), was obtained for the distorted structure.

In order to obtain a simplified microscopic understanding of the SOC induced magnetic

anisotropy and large spin wave gap in this half-filled AFM insulating system, we will consider a minimal three-orbital model involving the yz, xz, xy orbitals constituting the t_{2g} sector of the $5d$ orbitals. The role of the structural distortion will be incorporated through a hopping (bandwidth) asymmetry consistent with the orbital and directional asymmetry in the electron hopping terms as obtained from the electronic band structure comparison mentioned above.

A. Non-magnetic state

Including the local spin-orbit coupling and the band terms represented in the three-orbital basis ($yz\sigma, xz\sigma, xy\bar{\sigma}$), the free part of the Hamiltonian:

$$\mathcal{H}_{\text{SO}} + \mathcal{H}_{\text{band}} = \sum_{\mathbf{k}\sigma} \psi_{\mathbf{k}\sigma}^\dagger \begin{pmatrix} \mathcal{E}_{\mathbf{k}}^{yz} & i\sigma\frac{\lambda}{2} & -\sigma\frac{\lambda}{2} \\ -i\sigma\frac{\lambda}{2} & \mathcal{E}_{\mathbf{k}}^{xz} & i\frac{\lambda}{2} \\ -\sigma\frac{\lambda}{2} & -i\frac{\lambda}{2} & \mathcal{E}_{\mathbf{k}}^{xy} \end{pmatrix} \psi_{\mathbf{k}\sigma} \quad (1)$$

where $\mathcal{E}_{\mathbf{k}}^\mu$ are the band energies for the three orbitals $\mu = yz, xz, xy$, defined with respect to a common spin-orbital coordinate system. In the following it will be convenient to distinguish between the band energy contributions from hopping terms connecting opposite sublattices ($\epsilon_{\mathbf{k}}^\mu$) and same sublattice ($\epsilon_{\mathbf{k}}^{\mu'}$). In addition to the orbital-diagonal band terms above, hopping terms involving orbital mixing will be considered below.

B. AFM state and staggered field

Including the symmetry-breaking staggered fields $-s\boldsymbol{\sigma}\cdot\boldsymbol{\Delta}_\mu$ for the three orbitals $\mu = yz, xz, xy$, where $s = \pm 1$ for the two sublattices A/B, the staggered-field contribution:

$$\mathcal{H}_{\text{sf}} = \sum_{\mathbf{k}\sigma s} s\sigma\psi_{\mathbf{k}\sigma s}^\dagger \begin{pmatrix} -\Delta_{yz}^z & 0 & 0 \\ 0 & -\Delta_{xz}^z & 0 \\ 0 & 0 & +\Delta_{xy}^z \end{pmatrix} \psi_{\mathbf{k}\sigma s} \quad (2)$$

for ordering in the z direction. For general ordering direction with components $\boldsymbol{\Delta}_\mu = \Delta_\mu^x, \Delta_\mu^y, \Delta_\mu^z$ for orbital μ , the spin-space representation of the staggered field contribution:

$$\mathcal{H}_{\text{sf}} = \sum_{\mathbf{k}\sigma\sigma's\mu} \psi_{\mathbf{k}\sigma s\mu}^\dagger \left(-s\boldsymbol{\sigma}\cdot\boldsymbol{\Delta}_\mu \right)_{\sigma\sigma'} \psi_{\mathbf{k}\sigma's\mu} = \sum_{\mathbf{k}\sigma\sigma's\mu} s\psi_{\mathbf{k}\sigma s\mu}^\dagger \begin{pmatrix} -\Delta_\mu^z & -\Delta_\mu^x + i\Delta_\mu^y \\ -\Delta_\mu^x - i\Delta_\mu^y & \Delta_\mu^z \end{pmatrix}_{\sigma\sigma'} \psi_{\mathbf{k}\sigma's\mu}$$

(3)

Combining the SO, band, and staggered field terms, the total Hamiltonian is given below in the composite three-orbital, two-sublattice basis, showing the hopping terms connecting same and opposite sublattices, and the staggered field contribution (for z direction ordering). Also included are the hopping terms involving orbital mixing between the yz , xz and xy orbitals due to the structural distortion resulting from the octahedral rotation and tilting. Involving nearest-neighbor hopping, these orbital mixing terms are placed in the sublattice-off-diagonal ($s\bar{s}$) part of the Hamiltonian:

$$\begin{aligned} \mathcal{H}_{\text{SO}} + \mathcal{H}_{\text{band}} + \mathcal{H}_{\text{sf}} = & \sum_{\mathbf{k}\sigma s} \psi_{\mathbf{k}\sigma s}^\dagger \left[\begin{pmatrix} \epsilon_{\mathbf{k}}^{yz'} & i\sigma\frac{\lambda}{2} & -\sigma\frac{\lambda}{2} \\ -i\sigma\frac{\lambda}{2} & \epsilon_{\mathbf{k}}^{xz'} & i\frac{\lambda}{2} \\ -\sigma\frac{\lambda}{2} & -i\frac{\lambda}{2} & \epsilon_{\mathbf{k}}^{xy'} \end{pmatrix} - s\sigma \begin{pmatrix} \Delta_{yz}^z & 0 & 0 \\ 0 & \Delta_{xz}^z & 0 \\ 0 & 0 & -\Delta_{xy}^z \end{pmatrix} \right] \psi_{\mathbf{k}\sigma s} \\ & + \sum_{\mathbf{k}\sigma s} \psi_{\mathbf{k}\sigma s}^\dagger \begin{pmatrix} \epsilon_{\mathbf{k}}^{yz} & \epsilon_{\mathbf{k}}^{yz|xz} & \epsilon_{\mathbf{k}}^{yz|xy} \\ -\epsilon_{\mathbf{k}}^{yz|xz} & \epsilon_{\mathbf{k}}^{xz} & \epsilon_{\mathbf{k}}^{xz|xy} \\ -\epsilon_{\mathbf{k}}^{yz|xy} & -\epsilon_{\mathbf{k}}^{xz|xy} & \epsilon_{\mathbf{k}}^{xy} \end{pmatrix} \psi_{\mathbf{k}\sigma\bar{s}} \end{aligned} \quad (4)$$

The staggered fields Δ_{μ} are self-consistently determined from:

$$2\Delta_{\mu} = U_{\mu}\mathbf{m}_{\mu} + J_{\text{H}} \sum_{\nu \neq \mu} \mathbf{m}_{\nu} \quad (5)$$

in terms of the staggered magnetizations $\mathbf{m}_{\mu} = (m_{\mu}^x, m_{\mu}^y, m_{\mu}^z)$ for the three orbitals μ . The staggered field terms in the AFM state arise from the Hartree-Fock (HF) approximation of the electron interaction terms: $\sum_{i\mu} U_{\mu} n_{i\mu\uparrow} n_{i\mu\downarrow} - 2J_{\text{H}} \sum_{i,\mu \neq \nu} \mathbf{S}_{i\mu} \cdot \mathbf{S}_{i\nu}$, where U and J_{H} are the Hubbard and Hund's rule coupling terms, respectively. For general ordering direction with staggered field components $\Delta_{\mu} = (\Delta_{\mu}^x, \Delta_{\mu}^y, \Delta_{\mu}^z)$ for orbital μ , the staggered magnetization components ($\alpha = x, y, z$) are evaluated from:

$$[m_{\mu}^{\alpha}]_A = \frac{1}{N} \sum_{\mathbf{k}, l}^{E_{\mathbf{k}l} < E_{\text{F}}} \left(\phi_{\mathbf{k}l\mu}^{\uparrow*} \quad \phi_{\mathbf{k}l\mu}^{\downarrow*} \right)_A [\sigma^{\alpha}] \begin{pmatrix} \phi_{\mathbf{k}l\mu}^{\uparrow} \\ \phi_{\mathbf{k}l\mu}^{\downarrow} \end{pmatrix}_A = -[m_{\mu}^{\alpha}]_B \quad (6)$$

where $\phi_{\mathbf{k}l}$ are the eigenvectors of the total Hamiltonian $\mathcal{H}_{\text{SO}} + \mathcal{H}_{\text{band}} + \mathcal{H}_{\text{sf}}$, l is the branch label and N is the total number of \mathbf{k} states. In practice, it is easier to consider a given Δ and self-consistently determine the interaction strength U_{μ} from Eq. 5.

For straight Os-O-Os bonds (undistorted structure), all hopping terms between NN Os ions are orbital-diagonal with no orbital mixing. Due to twisting of Os-O-Os bonds associated with rotation and tilting of the OsO₆ octahedra in NaOsO₃, local cubic axis of OsO₆ octahedra are alternatively rotated, giving rise to small mixing between the yz , xz and xy orbitals. The effect of the structural distortion due to the octahedral rotation and tilting will be approximately incorporated through a hopping asymmetry between the orbitals, with slightly reduced bandwidth for the yz, xz orbitals compared to that for the xy orbital.

C. Tight-binding model

Corresponding to the hopping terms in the tight-binding representation, we will consider the band energy contributions in Eq. (4) for opposite ($\epsilon_{\mathbf{k}}^{\mu}$) and same ($\epsilon_{\mathbf{k}}^{\mu'}$) sublattices:

$$\begin{aligned}
\epsilon_{\mathbf{k}}^{xy} &= -4t_1 \cos(k_x/2) \cos(k_y/2) \\
\epsilon_{\mathbf{k}}^{xy'} &= -2t_2(\cos k_x + \cos k_y) + \epsilon_{xy} \\
\epsilon_{\mathbf{k}}^{yz} &= -2t_4[\cos\{(k_x - k_y)/2\} + \cos k_z] \\
\epsilon_{\mathbf{k}}^{yz'} &= -4t_2 \cos\{(k_x - k_y)/2\} \cos k_z \\
\epsilon_{\mathbf{k}}^{xz} &= -2t_4[\cos\{(k_x + k_y)/2\} + \cos k_z] \\
\epsilon_{\mathbf{k}}^{xz'} &= -4t_2 \cos\{(k_x + k_y)/2\} \cos k_z \\
\epsilon_{\mathbf{k}}^{yz|xz} &= -4t_{m1} \cos(k_x/2) \cos(k_y/2) \\
\epsilon_{\mathbf{k}}^{yz|xy} &= +\sqrt{2}t_{m2}[\cos\{(k_x + k_y)/2\} + 2 \cos\{(k_x - k_y)/2\} + \cos k_z] \\
\epsilon_{\mathbf{k}}^{xz|xy} &= -\sqrt{2}t_{m2}[2 \cos\{(k_x + k_y)/2\} + \cos\{(k_x - k_y)/2\} + \cos k_z]
\end{aligned} \tag{7}$$

Here t_1 and t_2 are the first and second neighbor hopping terms for the xy orbital, which has energy offset ϵ_{xy} relative to the degenerate yz/xz orbitals. For the yz and xz orbitals, t_4 and t_2 are the first and second neighbor hopping terms. Mixing between xz and yz orbitals and between xy and xz, yz orbitals is represented by the first neighbor hopping terms t_{m1} and t_{m2} , respectively. From the transformation of the hopping Hamiltonian matrix in the rotated basis, the orbital mixing hopping terms have been shown to be related to the OsO₆ octahedral rotation and tilting angles through $t_{m1} = V_{\pi}\theta_r = t_1\theta_r$ and $t_{m2} = V_{\pi}\theta_t/\sqrt{2} = t_1\theta_t/\sqrt{2}$ in the small angle approximation.¹¹

The case $t_4 = t_1$ and $t_{m1} = t_{m2} = 0$ corresponds to the undistorted structure (cubic

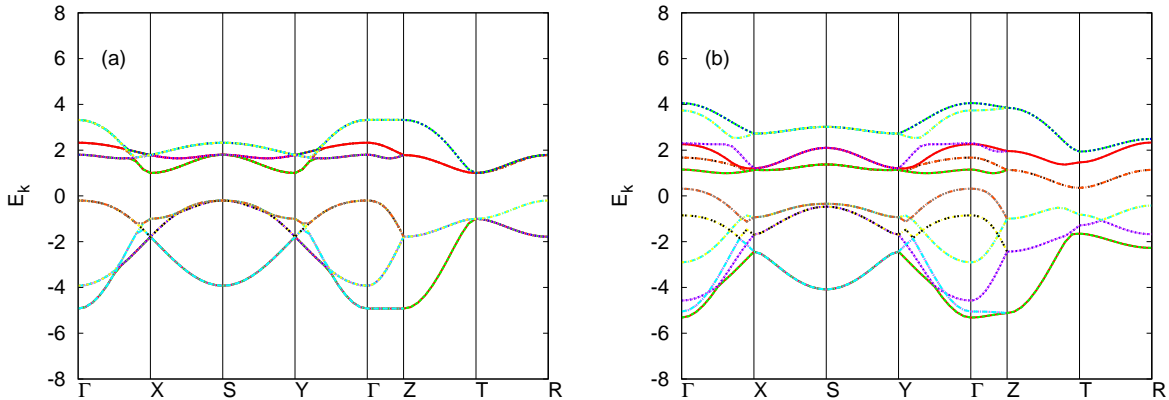


FIG. 1: Electronic band structure in the AFM state calculated from the minimal three-orbital model without (a) and with (b) SOC.

symmetry) with identical hopping terms for all three orbitals and no orbital mixing hopping terms. The effect of the structural distortion will be approximately incorporated through the hopping asymmetry $t_4 < t_1$, with slightly reduced bandwidth for the yz, xz orbitals compared to that for the xy orbital. This hopping asymmetry is broadly consistent with the detailed electronic band structure study carried out recently within the three-orbital model and comparison with DFT results for the distorted structure.¹¹ In the following, we will neglect the orbital mixing hopping terms t_{m1}, t_{m2} in order to focus on the role of the hopping asymmetry; effect of the mixing terms on magnetic anisotropy will be discussed in Sec. VI.

Figure 1 shows the calculated electronic band structure in the AFM state for the simplified three-orbital model without (a) and with (b) SOC ($\lambda = 1.3$). Here, the staggered field $\Delta = 1.0$, and the tight binding hopping parameter values $t_1, t_2, t_4, \epsilon_{xy} = 1.0, 0.2, 0.75, 0.0$, with the energy scale $t_1 = 400$ meV corresponding to the distorted structure,¹¹ which yields SOC ≈ 0.5 eV and $\Delta = 0.4$ eV. The separation of the energy bands into two groups of three above and three below the Fermi energy corresponds to the scenario where Hund's rule coupling dominates over spin-orbit coupling. As seen from Fig. 1(b), the strong SOC significantly reduces the indirect band gap. The AFM state insulating gap barely survives when SOC is included, resulting in a marginally insulating system. The calculated electronic band structure for the simplified three-orbital model is broadly consistent with first-principles calculations. For no SOC, the upper band minima are degenerate at X, Y, T, but the minimum at T becomes lowest when SOC is included.

III. SOC INDUCED MAGNETIC ANISOTROPY

The spin-orbit coupling terms can be written in spin space as:

$$\begin{aligned}
 H_{\text{SO}} = \sum_i \left[\left(\psi_{yz\uparrow}^\dagger \quad \psi_{yz\downarrow}^\dagger \right) (i\sigma_z \lambda/2) \begin{pmatrix} \psi_{xz\uparrow} \\ \psi_{xz\downarrow} \end{pmatrix} + \left(\psi_{xz\uparrow}^\dagger \quad \psi_{xz\downarrow}^\dagger \right) (i\sigma_x \lambda/2) \begin{pmatrix} \psi_{xy\uparrow} \\ \psi_{xy\downarrow} \end{pmatrix} \right. \\
 \left. + \left(\psi_{xy\uparrow}^\dagger \quad \psi_{xy\downarrow}^\dagger \right) (i\sigma_y \lambda/2) \begin{pmatrix} \psi_{yz\uparrow} \\ \psi_{yz\downarrow} \end{pmatrix} \right] \quad (8)
 \end{aligned}$$

which explicitly breaks the SU(2) spin-rotation symmetry. A strong-coupling expansion in terms of the spin-orbit coupling terms (Appendix A) explicitly shows the emergence of the anisotropic spin interactions. However, when all three contributions in Eq. (A2) are considered together, the magnetic anisotropy is expressed only when the magnetic moments are *not* orbitally independent, as seen from Eq. (A3). The hopping asymmetry $t_4 < t_1$ and the resulting magnetic moment asymmetry $m_{yz}, m_{xz} > m_{xy}$ is therefore an essential requirement in the minimal three-orbital model for the expression of the magnetic anisotropy.

In this section we discuss the resulting magnetic anisotropy and preferential ordering direction. We consider the (π, π, π) AFM state of the three-orbital model with SOC, and examine the ground state energy for the staggered field applied in x, y, z directions in spin space. For simplicity, we consider the same staggered field magnitude for all three orbitals. The AFM ground state energy was obtained by summing the HF level band energies for all occupied states. For vanishing SOC, the ground state energy was confirmed to be degenerate for all ordering directions. At finite SOC, variation of the ground state energy with the staggered field orientation explicitly shows the magnetic anisotropy corresponding to the spin-rotation symmetry breaking by SOC. As further discussed below, preferential magnetic ordering was obtained in the xy plane, corresponding to a single-ion anisotropy term $\sum_i DS_{iz}^2$ in an effective spin model with $D > 0$. A small hopping asymmetry between the yz and xz orbitals further allows for easy axis selection within the xy plane.

The strong magnetic anisotropy induced by SOC is shown in Fig. 2 through the variation of the ground state energy with the staggered field orientation. In the absence of SOC, the ground state energy is independent of θ . The ground state energy is strongly reduced when SOC is turned on [Fig. 3], the reduction being weakly dependent on the staggered field orientation. It is this weak dependence on the staggered field orientation which gives rise to the magnetic anisotropy. The strong coupling expansion carried out to second order in

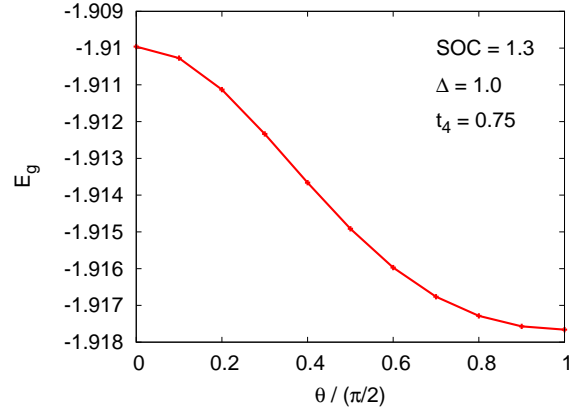


FIG. 2: SOC induced magnetic anisotropy shown by significant dependence of electronic ground state energy (per state) with the staggered field orientation θ from the S_z axis. The easy-plane anisotropy and the $\cos^2 \theta$ dependence correspond to the single-ion anisotropy term DS_{iz}^2 .

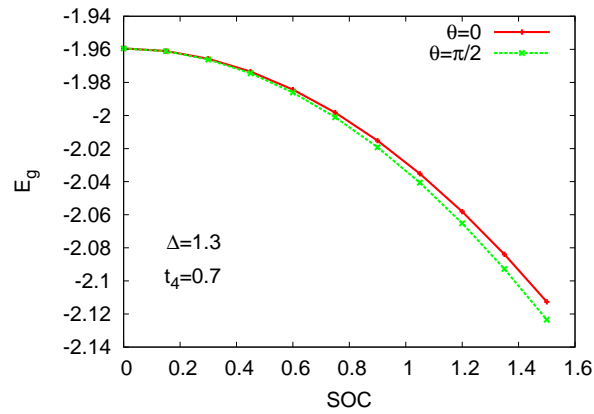


FIG. 3: SOC induced reduction in the electronic ground state energy (per state) for two different orientations of the staggered field: along S_z direction ($\theta = 0$) and S_x direction ($\theta = \pi/2$).

SOC (Appendix A) accounts for the $O(\lambda^2)$ reduction in the ground state energy with SOC [Fig. 3], and also the weak dependence on the staggered field orientation.

The magnetic anisotropy energy [Fig. 4(a)] obtained as the difference $\Delta E_g = E_g(z) - E_g(x)$ between the ground state energies (per state) for z and x orientations of the staggered field varies as λ^2 . As mentioned earlier, the magnetic anisotropy energy crucially depends on the hopping asymmetry between the xy and yz/xz orbitals, as explicitly shown in Fig. 4(b). The origin of this dependence of the magnetic anisotropy energy on the hopping asymmetry is related to the corresponding magnetic moment asymmetry, resulting in finite

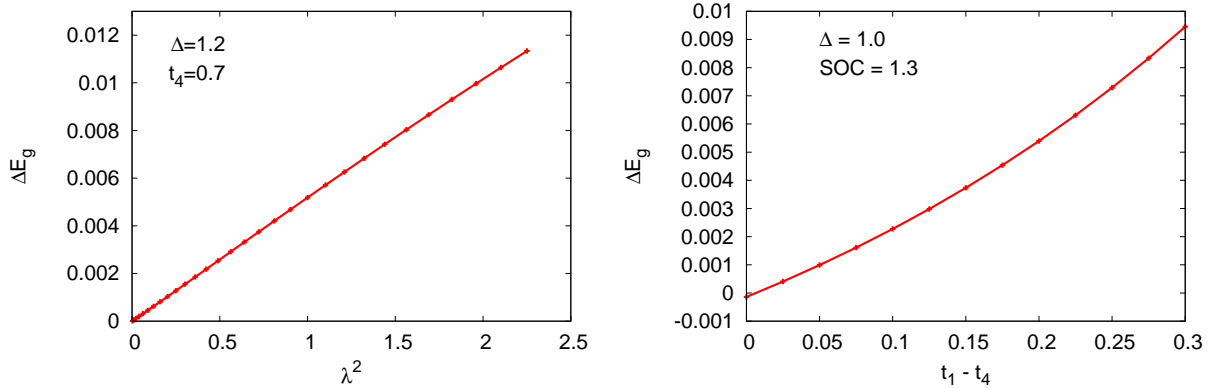


FIG. 4: Variation of the magnetic anisotropy energy $\Delta E_g = E_g(z) - E_g(x)$ with (a) the square of the spin-orbit coupling and (b) the hopping asymmetry $t_1 - t_4$ between the xy and the yz/xz orbitals.

orbital-Kitaev anisotropy, as discussed in the Appendix A.

Effective single-ion anisotropy

The magnetic anisotropy energy $\Delta E_g = E_g(z) - E_g(x)$ obtained above is in quantitative agreement with the effective single-ion anisotropy energy considered phenomenologically in recent spin wave calculations using localized spin models.² From the calculated magnetic anisotropy energy $\Delta E_g \approx 0.0075$ (per state) for $\text{SOC} = 1.3$ as in Fig. 2, and using the energy scale $t_1 = 400$ meV, we obtain the effective single-ion anisotropy energy:

$$\Delta E_{\text{sia}} = 3 \times 0.0075 \times 400 \text{ meV} = 9 \text{ meV} \quad (9)$$

where the factor 3 corresponding to the three t_{2g} orbitals per Osmium accounts for the conversion from average energy per state to average energy per ion. The above value is in agreement with that obtained from the single-ion anisotropy term $\Delta E_{\text{sia}} = DS_{iz}^2$ for $D = 4$ meV and $S = 3/2$ as considered phenomenologically in localized spin models.²

IV. INTRA-SITE MAGNETIC FRUSTRATION AND ORBITAL 120° STATE

The collinear AFM ordering discussed above with local magnetic moments for all three orbitals aligned parallel along some direction in the $x-y$ plane, although energetically better

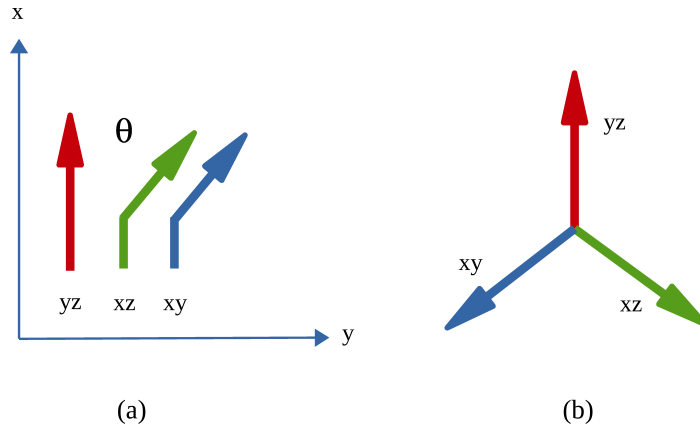


FIG. 5: (a) Local magnetic moment orientations for the three orbitals in the orbital canted state, and (b) the orbital 120° state after the transformation described in Appendix B for $\theta = \pi/3$.

than ordering in the z direction, is not the optimal configuration in the absence of Hund's coupling. This is inferred from the spin wave analysis (discussed in the next section) which yields negative energy mode, and the instability eigenvector of the $[\chi^0]$ matrix indicates nearly equal transverse spin twisting for the xz and xy orbital moments while keeping the yz orbital moment unchanged.

Correspondingly, the AFM state energy was reevaluated for the configuration shown in Fig. 5 where two of the orbital moments are canted with respect to the third by angle θ . The results for the ground state energy are shown in Fig. 6 for two cases: (i) the yz orbital moment aligned along x direction and the xz, xy orbital moments canted by angle θ in the y direction [Fig. 5(a)] and (ii) the xy orbital moment aligned along z direction and the yz, xz orbital moments canted by angle θ in the x direction. These two configurations are labelled x and z respectively in Fig. 6. The results clearly show an energy minimum at canting angle $\theta \approx \pi/3$. The optimal canting angle is exactly $\theta = \pi/3$ in the absence of hopping asymmetry ($t_4 = t_1$), and the two configurations are degenerate.

The above result of ground state energy minimum at orbital canting angle $\theta \approx \pi/3$ can be readily understood from the anisotropic (orbital-Kitaev type) spin interaction terms generated in the strong-coupling expansion (Appendix A). Assuming equal magnitudes for

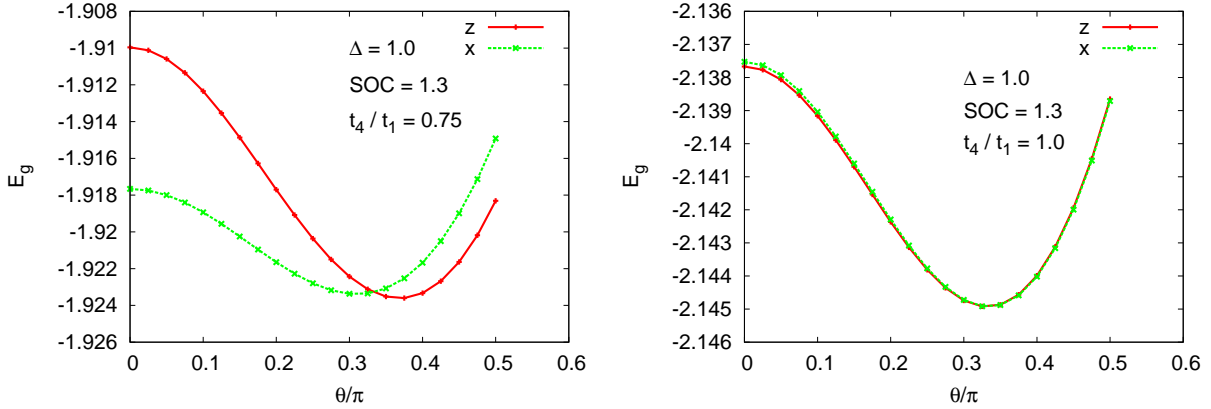


FIG. 6: (a) Variation of the band AFM state energy with angle θ in the orbital canted state (see Fig. 5) showing the energy minimum at $\theta \approx \pi/3$. (b) The optimal canting angle is exactly $\theta = \pi/3$ in the absence of hopping asymmetry, and the two configurations are degenerate.

the magnetic moments S_μ , the energy for the orbital canted configuration:

$$\begin{aligned} E_g &= \frac{4(\lambda/2)^2}{U} S_\mu^2 [(-\cos \theta) + (\cos^2 \theta - \sin^2 \theta) + (-\cos \theta)] \\ &= \frac{4(\lambda/2)^2}{U} S_\mu^2 [\cos 2\theta - 2\cos \theta] \end{aligned} \quad (10)$$

corresponding to the three terms in Eq. (A2), minimization of which yields $\theta = \pi/3$. Furthermore, the minimum ground state energy in the orbital canted state is $-3/2$ (in units of λ^2/U), with equal contribution from each of the three terms, whereas the minimum energy in the collinear AFM state with magnetic moments for all three orbitals aligned parallel is -1 in same units.

Now, if the Hund's coupling term:

$$-J_H \sum_{\mu \neq \nu} \mathbf{S}_\mu \cdot \mathbf{S}_\nu \approx -2J_H S_\mu^2 \cos \theta \quad (11)$$

is included in the energy consideration for the orbital canted state, the ground state energy is modified to:

$$E_g = J_\lambda S_\mu^2 [\cos 2\theta - 2(1 + r_H) \cos \theta] \quad (12)$$

where $J_\lambda \equiv 4(\lambda/2)^2/U$ and the ratio $r_H = J_H/J_\lambda$. The energy minimum condition is now modified to:

$$\cos \theta = \frac{1 + r_H}{2} \quad (\text{or } \sin \theta = 0) \quad (13)$$

and the optimal canting angle decreases from $\theta = \pi/3$ at $r_H = 0$ to $\theta = 0$ for $r_H \geq 1$, as expected with increasing Hund's coupling.

The same reduction in the canting angle due to Hund's coupling can be seen from the staggered field equations:

$$2\Delta_{\alpha} = U\mathbf{m}_{\alpha} + J_H \sum_{\beta \neq \alpha} \mathbf{m}_{\beta} \quad (14)$$

within a self-consistent iteration scheme at the HF level. Starting with the canted configuration as shown in Fig. 5, the staggered field for the yz orbital and similarly for the xz, xy orbitals will generate, due to the Hund's coupling term, components in the normal directions to the moments, which will reduce the canting angle θ between these moments.

The significant role of Hund's coupling on magnetic anisotropy is evident from Fig. 6(a). In the absence of J_H , the energy minima at canting angle $\theta \approx \pi/3$ are nearly degenerate for the two configurations labelled x and z . However, with canting angle reduced to zero at sufficiently strong J_H , the magnetic anisotropy becomes effective, favouring ordering in the x direction as compared to z direction.

V. SPIN WAVE EXCITATIONS

Due to the spin mixing terms in the Hamiltonian (Eqs. 1,3), spin is not a good quantum number, and we therefore use the method developed earlier for the 120° (non-collinear) ordering on the triangular lattice to investigate spin waves.¹³ In the (π, π, π) AFM ground state $|\Psi_0\rangle$ of the three-orbital model as discussed above, we consider the time-ordered transverse spin fluctuation propagator in the composite orbital-sublattice basis:

$$\chi^{-+}(\mathbf{q}, \omega) = \int dt \sum_i e^{i\omega(t-t')} e^{-i\mathbf{q}\cdot(\mathbf{r}_i - \mathbf{r}_j)} \times \langle \Psi_0 | T[S_{i\mu}^{\alpha}(t) S_{j\nu}^{\beta}(t')] | \Psi_0 \rangle \quad (15)$$

involving the spin operators at lattice sites i, j for orbitals μ, ν and components $\alpha, \beta = x, y, z$. In the random phase approximation (RPA), the spin wave propagator is obtained as:

$$[\chi_{\text{RPA}}^{-+}(\mathbf{q}, \omega)] = \frac{[\chi^0(\mathbf{q}, \omega)]}{\mathbf{1} - [U][\chi^0(\mathbf{q}, \omega)]} = \frac{1}{[U] - [U][\chi^0(\mathbf{q}, \omega)][U]} - \frac{1}{[U]} \quad (16)$$

where the local interaction matrix $[U]$ in the orbital-sublattice basis is given by: $[U]_{\mu\nu} = U_{\mu}$ for $\mu = \nu$ (intra-orbital Hubbard term) and $[U]_{\mu\nu} = J_H$ for $\mu \neq \nu$ (inter-orbital Hund's

coupling term). The bare particle-hole propagator:

$$[\chi^0(\mathbf{q}, \omega)]_{ab}^{\alpha\beta} = \frac{1}{2} \sum_{\mathbf{k}, l, m} \left[\frac{\langle \phi_{\mathbf{k}, l} | \sigma^\alpha | \phi_{\mathbf{k}-\mathbf{q}, m} \rangle_a \langle \phi_{\mathbf{k}-\mathbf{q}, m} | \sigma^\beta | \phi_{\mathbf{k}, l} \rangle_b}{E_{\mathbf{k}-\mathbf{q}, m}^+ - E_{\mathbf{k}, l}^- + \omega - i\eta} + \frac{\langle \phi_{\mathbf{k}, l} | \sigma^\alpha | \phi_{\mathbf{k}-\mathbf{q}, m} \rangle_a \langle \phi_{\mathbf{k}-\mathbf{q}, m} | \sigma^\beta | \phi_{\mathbf{k}, l} \rangle_b}{E_{\mathbf{k}, l}^+ - E_{\mathbf{k}-\mathbf{q}, m}^- + \omega - i\eta} \right] \quad (17)$$

was evaluated in the orbital-sublattice basis by integrating out the fermions in the AFM state. Here $E_{\mathbf{k}}$ and $\phi_{\mathbf{k}}$ are the eigenvalues and eigenvectors of the Hamiltonian matrix, the indices a, b in the composite orbital-sublattice basis run through 1-6, and l, m indicate the six eigenvalue branches. The superscripts $+$ ($-$) refer to particle (hole) energies above (below) the Fermi energy.

Before presenting the spin wave calculation results, we try to anticipate the role of Hund's coupling on magnetic excitations in the AFM state. In the absence of Hund's coupling, the ground state energy was shown to have a minimum at finite canting angle $\theta \approx \pi/3$ between the orbital magnetic moments [Fig. 6(a)]. The orbitally collinear AFM state ($\theta = 0$) with magnetic moments for all three orbitals aligned parallel (in the x direction) therefore does not correspond to the ground state configuration, and spin waves should therefore yield negative energy mode representing the instability of the orbitally collinear AFM state. The optimal canting angle decreases when Hund's coupling is turned on, approaching $\theta = 0$ for sufficiently strong J_H as discussed in Sec. IV. The orbitally collinear (uncanted) AFM state ($\theta = 0$) with moments ordered in the x direction now does represent the ground state, and spin waves should therefore yield gapless mode corresponding to transverse fluctuations in the y direction, whereas fluctuations in the z direction should be gapped.

Calculated spin wave energies in the uncanted AFM state with magnetic moments for all three orbitals oriented along the x direction are shown in Fig. 7 for the two cases: with and without Hund's coupling. Here the staggered field $\Delta = 1$, SOC = 1.3, $t_1 = 1.0$, $t_2 = 0.2$, and $t_4 = 0.7$, with the energy scale $t_1 = 400$ meV. In the case $J_H = 0$, the negative energy of the y -fluctuation mode for $q = 0$ confirms the instability as expected from Fig. 6(a) which shows that the uncanted AFM state ($\theta = 0$) is not the lowest energy state. However, for sufficiently strong Hund's coupling, when the optimal canting angle decreases to $\theta = 0$, the finite magnetic anisotropy energy corresponding to the ground state energy difference [Fig. 6(a)] for magnetic orderings in the x and z directions accounts for the finite spin wave gap ≈ 50 meV seen in Fig. 7(a) for the z fluctuation mode.

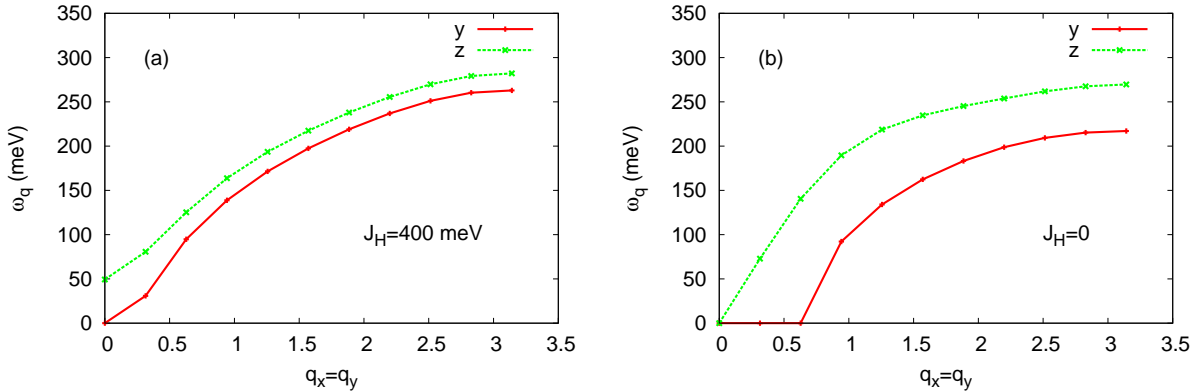


FIG. 7: Calculated spin wave energies in the staggered AFM state with all orbital moments along x direction for the two cases: (a) with and (b) without Hund's coupling. The finite spin wave gap ≈ 50 meV for the z fluctuation mode in (a) corresponds to the finite magnetic anisotropy energy at $\theta = 0$ in Fig. 6(a). The instability of the y fluctuation mode in (b) corresponds to the ground state energy minimum not at $\theta = 0$ but at finite canting angle in the absence of Hund's coupling.

VI. EFFECT OF THE ORBITAL ENERGY OFFSET

The xy orbital density (n_{xy}) is found to decrease in magnitude as the staggered field orientation changes from z direction ($\theta = 0$) to x direction ($\theta = \pi/2$). This suggests that the xy orbital energy offset ϵ_{xy} (with respect to the degenerate xz/yz orbitals) should also contribute to the magnetic anisotropy energy, with positive ϵ_{xy} favouring x ordering. The x - y symmetry of the three-orbital model should result in easy $x - y$ plane in general. Fig. 8 shows the ground state energy variation with θ for finite ϵ_{xy} . For the parameters shown, the magnetic anisotropy energy $\Delta E_g = E_g(z) - E_g(x) \approx 0.008$ (similar to Fig. 2), with roughly equal contributions from the orbital energy offset ϵ_{xy} and the hopping asymmetry $t_4 < t_1$ when considered individually. The staggered field magnitudes were taken as $\Delta_{yz} = \Delta_{xz} = 1.1$ and $\Delta_{xy} = 1.0$ such that $U_\mu \approx 3.5$ for all three orbitals ($J_H = 0$).

Similar magnitude of the magnetic anisotropy energy was obtained with realistic hopping parameters as obtained from a recent electronic band structure comparison using DFT and the three orbital model.¹¹ This calculation with realistic hopping parameters included the orbital mixing hopping terms (t_{m1}, t_{m2}) as given in Eq. 7. We did not find any enhancement in the magnetic anisotropy energy due to the orbital mixing terms in either case.

The origin of the reduction in n_{xy} with staggered field rotation is as follows. In the

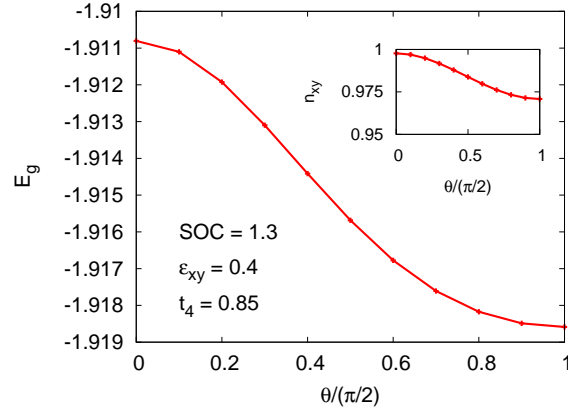


FIG. 8: SOC induced magnetic anisotropy in presence of both hopping asymmetry $t_4 < t_1$ and orbital energy offset ϵ_{xy} , as shown by the dependence of the electronic ground state energy (per state) with the staggered field orientation θ from the S_z axis. Inset shows the small reduction in the xy orbital density with orientation θ .

atomic limit, evolution of the SOC-split energy levels with increasing exchange field Δ has been studied.¹¹ In the $\Delta \rightarrow 0$ limit, the t_{2g} levels are split into the $J = 1/2$ doublet and the $J = 3/2$ quartet, and the total electron densities in the three lowest-energy ($J = 3/2$) levels are: $n_{xy} = 8/6$ and $n_{yz} = n_{xz} = 5/6$.¹² Due to progressive suppression of the SOC-induced spin-orbital entanglement, the density disparity decreases with increasing Δ . However, n_{xy} remains greater than n_{yz}, n_{xz} for finite Δ , even when hopping terms are included. Thus, for z orientation of the staggered field, $n_{xy} > n_{yz}, n_{xz}$, as indeed confirmed from the three-band model calculation. Now, rotating the staggered field from z to x direction is equivalent to spin space rotation by angle $\pi/2$ about the y axis, under which the orbitals transform as: $xz \rightarrow xz$, $yz \rightarrow xy$, and $xy \rightarrow yz$. The interchange of the yz and xy orbitals implies that $n_{xy} < n_{yz}$ for x orientation of the staggered field.

The above analysis highlights the importance of residual $J = 3/2$ character of lower band states and weak correlation in the magnetic anisotropy effect arising due to the coupling of the xy orbital density change $n_{xy}(z) - n_{xy}(x)$ with the tetragonal distortion-induced xy orbital energy offset ϵ_{xy} . Recent RIXS studies of the $5d^3$ systems $\text{Ca}_3\text{LiOsO}_6$ and Ba_2YOsO_6 have revealed evidence of the spin-orbit entangled $J = 3/2$ character of the electronic ground state.⁵

VII. CONCLUSIONS

Magnetic orderings, ground state energies, and excitations were investigated in the AFM state of a minimal three-orbital model at half filling with strong spin-orbit coupling. Asymmetry in the hopping terms for the three orbitals yz, xz, xy (associated with the OsO_6 octahedral tilting and rotation), resulting in asymmetry in the magnetic moments, was shown to be an essential ingredient in the minimal three-orbital model in order to understand the SOC induced magnetic anisotropy and large spin wave gap observed in the weakly correlated $5d^3$ compound NaOsO_3 involving competition between SOC, Hund's coupling, and the staggered field, all having comparable energy scales. A novel orbital canted state stabilized by the intrasite magnetic frustration effect due to the SOC-induced anisotropic (orbital-Kitaev) spin interactions was presented. Restoration of the orbitally collinear AFM state by Hund's coupling was shown to be instrumental in the expression of the magnetic anisotropy and the large spin wave gap.

The residual $J = 3/2$ character of the lower band states resulting from the combined SOC and electron interaction effects was found to exhibit a signature effect of reduction in the density n_{xy} with staggered field rotation from z to x direction. Coupling of this density change with the xy orbital energy offset ϵ_{xy} was therefore found to also contribute significantly to the magnetic anisotropy energy, and a smaller hopping asymmetry is thus sufficient to generate the required magnetic anisotropy energy for positive ϵ_{xy} . Similar magnitude of the magnetic anisotropy energy was obtained with realistic hopping parameters as obtained from a recent electronic band structure comparison using DFT and the three orbital model.

Appendix A: SOC-induced anisotropic spin interactions

The spin-orbit coupling terms can be written in spin space as:

$$\begin{aligned}
 H_{\text{SO}} = \sum_i & \left[\begin{aligned} & \left(\psi_{yz\uparrow}^\dagger \quad \psi_{yz\downarrow}^\dagger \right) \left(i\sigma_z \lambda / 2 \right) \begin{pmatrix} \psi_{xz\uparrow} \\ \psi_{xz\downarrow} \end{pmatrix} + \left(\psi_{xz\uparrow}^\dagger \quad \psi_{xz\downarrow}^\dagger \right) \left(i\sigma_x \lambda / 2 \right) \begin{pmatrix} \psi_{xy\uparrow} \\ \psi_{xy\downarrow} \end{pmatrix} \\ & + \left(\psi_{xy\uparrow}^\dagger \quad \psi_{xy\downarrow}^\dagger \right) \left(i\sigma_y \lambda / 2 \right) \begin{pmatrix} \psi_{yz\uparrow} \\ \psi_{yz\downarrow} \end{pmatrix} \end{aligned} \right] \quad (\text{A1})
 \end{aligned}$$

which explicitly shows the SU(2) spin-rotation symmetry breaking. Here we discuss the resulting magnetic anisotropy and preferential magnetic ordering direction. For this purpose, we perform a strong-coupling expansion as for the SOC-induced spin-dependent hopping terms of the form $i\sigma \cdot \mathbf{t}'_{ij}$, which yield the Kitaev type anisotropic spin interactions.¹⁴

As the three orbital ‘‘hopping’’ terms are of similar form as spin-dependent hopping, carrying out the strong-coupling expansion to second order in λ , we obtain similar anisotropic spin interactions:

$$H_{\text{eff}}^{(2)}(i) = \frac{4(\lambda/2)^2}{U} \left(\begin{aligned} & [S_{yz}^z S_{xz}^z - (S_{yz}^x S_{xz}^x + S_{yz}^y S_{xz}^y) - n_{yz} n_{xz}] \\ & + [S_{xz}^x S_{xy}^x - (S_{xz}^y S_{xy}^y + S_{xz}^z S_{xy}^z) - n_{xz} n_{xy}] \\ & + [S_{xy}^y S_{yz}^y - (S_{xy}^z S_{yz}^z + S_{xy}^x S_{yz}^x) - n_{xy} n_{yz}] \end{aligned} \right) \quad (\text{A2})$$

which are, it should be emphasized, local (intra-site) interactions between the magnetic moments for the three orbitals at site i . Assuming the local magnetic moments \mathbf{S}_μ to be independent of the orbital index μ , and similarly for the densities n_μ , we obtain:

$$H_{\text{eff}}^{(2)}(i) = -\frac{4(\lambda/2)^2}{U} [\mathbf{S} \cdot \mathbf{S} + 3n^2] \quad (\text{A3})$$

which accounts for the reduction of order (λ^2/U) in the ground state energy with the SOC strength λ , as seen in Fig. 3. The weak orbital dependence of the magnetic moments accounts for the small variation in the ground state energy with staggered field orientation, which is the source of the magnetic anisotropy. If the magnetic moment S_{xy} for the xy orbital is slightly smaller than for the xz, yz orbitals, and assuming parallel alignment of the magnetic moments for the three orbitals due to Hund’s coupling, the term in the first line of Eq. A2 dominates, resulting in preferred ordering in the xy plane. Within an equivalent spin model, this would correspond to the single ion anisotropy term DS_{iz}^2 with positive D .

The preferred magnetic ordering direction within the xy plane can be further selected if the degeneracy between the yz and xz magnetic moments is lifted. Considering only the $x - y$ components of the magnetic moments \mathbf{S}_μ in Eq. A2, we have:

$$H_{\text{eff}}^{(2)}(i) = \frac{4(\lambda/2)^2}{U} \left(-\mathbf{S}_{yz} \cdot \mathbf{S}_{xz} + S_{xy}^x (S_{xz}^x - S_{yz}^x) + S_{xy}^y (S_{yz}^y - S_{xz}^y) \right) \quad (\text{A4})$$

which clearly shows x (y) to be the preferred ordering direction if the moment S_{yz} is greater (less) than the moment S_{xz} . It should be noted that, in the absence of sufficiently strong Hund’s coupling, the AFM state with all three local magnetic moments \mathbf{S}_μ aligned parallel

does not correspond to the lowest-energy state due to the intra-site magnetic frustration effect, as discussed below.

Appendix B: Spin transformation, magnetic frustration, and orbital 120° state

Under the transformation:

$$\begin{aligned}\mathbf{S}_{yz} &\rightarrow \mathbf{S}'_{yz} = (S_{yz}^x, -S_{yz}^y, -S_{yz}^z) \\ \mathbf{S}_{xz} &\rightarrow \mathbf{S}'_{xz} = (-S_{xz}^x, S_{xz}^y, -S_{xz}^z) \\ \mathbf{S}_{xy} &\rightarrow \mathbf{S}'_{xy} = (-S_{xy}^x, -S_{xy}^y, S_{xy}^z)\end{aligned}\tag{B1}$$

where two spin components are reversed for each orbital in cyclic fashion, the effective interaction Hamiltonian in Eq. A2 transforms to the isotropic form:

$$H_{\text{eff}}^{(2)}(i) = \frac{4(\lambda/2)^2}{U} \sum_{\mu \neq \nu} (\mathbf{S}'_{\mu} \cdot \mathbf{S}'_{\nu} - n_{\mu} n_{\nu})\tag{B2}$$

which highlights the SOC induced magnetic frustration between the three local magnetic moments \mathbf{S}_{μ} . In analogy with the 120° state of the geometrically frustrated triangular lattice AFM, the orbital canted state shown in Fig. 5(a) corresponds, for $\theta = \pi/3$, to an orbital 120° state in which the transformed magnetic moments \mathbf{S}'_{yz} , \mathbf{S}'_{xz} , \mathbf{S}'_{xy} are oriented at 120° with respect to each other, as shown in Fig. 5(b).

This intra-site magnetic frustration and canting tendency of the orbital magnetic moments persists even when hopping is turned on, as is evident from Fig. 6, showing the energy minimum at canting angle $\theta \approx \pi/3$ in the band AFM state.

Acknowledgement

We thank the U.S. Department of Energy, Office of Basic Energy Sciences, Division of Materials Sciences and Engineering (GrantNo. DE-FG02-00ER45818) for financial support. AS acknowledges sponsorship grant from the Alexander von Humboldt Foundation for a research stay at IFW Dresden.

-
- ¹ S. Calder, V. O. Garlea, D. F. McMorrow, M. D. Lumsden, M. B. Stone, J. C. Lang, J.-W. Kim, J. A. Schlueter, Y. G. Shi, K. Yamaura, Y. S. Sun, Y. Tsujimoto, and A. D. Christianson, *Phys. Rev. Lett.* **108**, 257209 (2012).
 - ² S. Calder, J. G. Vale, N. Bogdanov, C. Donnerer, D. Pincini, M. Moretti Sala, X. Liu, M. H. Upton, D. Casa, Y. G. Shi, Y. Tsujimoto, K. Yamaura, J. P. Hill, J. van den Brink, D. F. McMorrow, and A. D. Christianson, *Phys. Rev. B* **95**, 020413(R) (2017).
 - ³ E. Kermarrec, C. A. Marjerrison, C. M. Thompson, D. D. Maharaj, K. Levin, S. Kroeker, G. E. Granroth, R. Flacau, Z. Yamani, J. E. Greedan, and B. D. Gaulin, *Phys. Rev. B* **91**, 075133 (2015).
 - ⁴ A. E. Taylor, R. Morrow, R. S. Fishman, S. Calder, A. I. Kolesnikov, M. D. Lumsden, P. M. Woodward, and A. D. Christianson, *Phys. Rev. B* **93**, 220408(R) (2016).
 - ⁵ A. E. Taylor, S. Calder, R. Morrow, H. L. Feng, M. H. Upton, M. D. Lumsden, K. Yamaura, P. M. Woodward, and A. D. Christianson, *Phys. Rev. Lett.* **118**, 207202 (2017).
 - ⁶ S. Calder, J.G. Vale, N.A. Bogdanov, X. Liu, C. Donnerer, M.H. Upton, D. Casa, A.H. Said, M.D. Lumsden, Z. Zhao, J.-Q. Yan, D. Mandrus, S. Nishimoto, J. van den Brink, J.P. Hill, D.F. McMorrow, and A.D. Christianson, *Nat. Commun.* **7**, 11651 (2016).
 - ⁷ Y. Du, X. Wan, L. Sheng, J. Dong, and S. Y. Savrasov, *Phys. Rev. B* **85**, 174424 (2012).
 - ⁸ M.-C. Jung, Y.-J. Song, K.-W. Lee, and W. E. Pickett, *Phys. Rev. B* **87**, 115119 (2013).
 - ⁹ Z. Ali, A. Sattar, S. J. Asadabadi, and I. Ahmad, *J. Phys. & Chem. Solids* **86**, 114 (2015).
 - ¹⁰ R. Morrow, K. Samanta, T. Saha Dasgupta, J. Xiong, J. W. Freeland, D. Haskel, and P. M. Woodward, *Chem. Mater.* **28**, 3666 (2016).
 - ¹¹ S. Mohapatra, C. Bhandari, S. Satpathy, and A. Singh, arXiv:1710.09597 (2017).
 - ¹² S. Mohapatra, J. van den Brink, and A. Singh, *Phys. Rev. B* **95**, 094435 (2017).
 - ¹³ A. Singh, *Phys. Rev. B* **71**, 214406 (2005).
 - ¹⁴ S. Mohapatra and A. Singh, arXiv:1712.00198 (2017).